Enhanced generation of charge-dependent second-order sideband and high-sensitivity charge sensors in a gain-cavity-assisted optomechanical system

Ling Li, Wen-Xing Yang,* Yuexin Zhang, and Tao Shui
Department of Physics, Southeast University, Nanjing 210096, China

Ai-Xi Chen†
Department of Physics, Zhejiang Sci-Tech University, Hangzhou 310018, China

Zhongming Jiang
High School Affiliated to Nanjing Normal University Jiangning Campus, Nanjing 211102, China

(Received 2 September 2018; published 26 December 2018)

We theoretically investigate the enhanced charge-dependent generation of the optical second-order sidebands (OSS) in a gain-cavity-assisted optomechanical (GCAOM) system coupled to a charged object. The hybrid optomechanical system is coherently driven by an external two-tone laser field which consists of a continuous-wave pump field and a pulsed probe field. Beyond the conventional linearized description of optomechanical interactions, the nonlinear optomechanical interactions are included in the Heisenberg-Langevin equations and are treated analytically by means of the perturbation method. It is shown that an assisted gain cavity can significantly enhance the OSS generation and can also lead to higher charge dependence of the output OSS spectrum than that achieved from a lossy cavity optomechanical system. Subsequently we discuss the application of such a GCAOM system as a family of high-sensitivity sensor for measuring the charges. Using experimentally achievable parameters, we identify the conditions under which the assisted gain cavity allows us to enhance the OSS generation and improve sensitivity of the sensor beyond what is achievable in a lossy cavity optomechanical system. The present investigation may provide a route toward modulating the nonlinear optical properties of the electro-optic hybrid system, as well as to guide the design of sensitive devices.

DOI: 10.1103/PhysRevA.98.063840

I. INTRODUCTION

Cavity optomechanics is a branch of physics which focuses on the interaction between light and mechanical resonator (MR) via radiation pressure with low-energy scales [1–7]. Cavity optomechanics have become a rapidly growing research field and have led to diverse applications in recent years, such as control of output spectra of light exotically [8–12], precision measurement [13–15], force sensors [16,17], and others [18–20]. A typical example for the control of output spectra is the optomechanically induced transparency (OMIT) [21,22], which is an analog of electromagnetically induced transparency (EIT) in atom gas [23] and can be well understood through the linearization of optomechanical interactions. The precision measurement using the optomechanical interaction is usually carried out via the correlations between the measured quantities and output spectra. An electric interaction has been introduced to a cavity optomechanical system and the electrical charge-dependent effect of OMIT has been studied [24]. Furthermore, a potential scheme to precisely measure the charge number of small charged objects based on OMIT has been proposed in an optomechanical system [24,25].

In addition to the studies of the linearized dynamics of the optomechanical interaction [26,27], there has been significant research activity on nonlinear optomechanical interactions [28]. These studies of nonlinear optomechanical interactions have aroused a lot of interesting topics in cavity optomechanics, such as second-order and higher-order sideband generation [29–31], optical frequency comb [32], optical solitons [33,34], and chaos [35]. The perturbative [36] and nonperturbative [37] methods for describing the nonlinear optomechanical interaction has been proposed. The spectral components of signal field at the second-order and higher-order sidebands have been predicted and analyzed, which exhibits the prominent feature of nonlinear OMIT [38,39]. It has been displayed that the nonlinear OMIT at the second-order mechanical sideband enables it to be an effective candidate for the precision measurement of the average phonon number of mechanical oscillator [40]. Furthermore, by including the electric interaction in the optomechanical system, several works have shown that the optical second-order sideband exhibited more sensitivity to electrical charges than the conventional linearized transmission spectra [24] and enabled an all-optical sensor for the measurement of charges with higher precision [41,42].

In this paper, we show that nonlinear optomechanical interaction can be modified by an assisted gain cavity to enable enhancement of the charge-dependent optical second-order sidebands (OSS) generation in an optomechanical system

*wenxingyang2@126.com
†aixichen@zstu.edu.cn

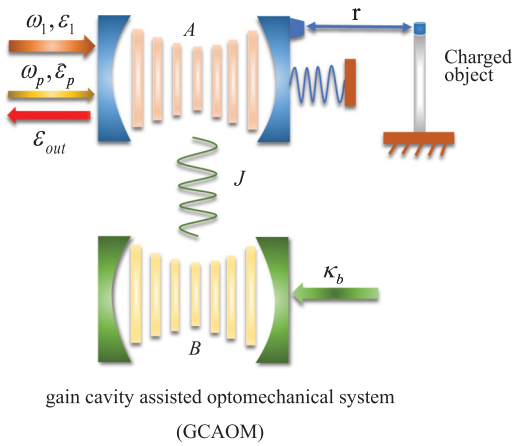

FIG. 1. Schematic diagram of a gain-cavity-assisted optomechanical (GCAOM) system, which consists of a lossy cavity optomechanical system and a gain cavity as well as a charged object. The lossy cavity optomechanical system is coupled to the gain cavity by the photon hopping, and the coupling strength J can be adjusted by changing the distant between the loss and gain cavities. The charged MR is coupled to the charged object through the Coulomb interaction. The hybrid system is driven by a strong pump field and a weak probe field through the lossy cavity.

coupled to a charged object. Unlike the linearized description of optomechanical interactions [43], the nonlinear interactions between cavity field and the MR are treated analytically by means of the perturbation method. We find that optical nonlinearity arising from nonlinear optomechanical interaction can be modified by the assisted gain cavity and the electric interaction, which results in the enhancement of the OSS and the highly sensitive charge dependence of the OSS spectrum. Thus the highly sensitive charge-dependent effects of the OSS can be used to devise a type of high-sensitivity optical sensor for measuring the charges. Using experimentally achievable parameters, we identify the conditions that are the optimal sensitivity of the sensor beyond what is achievable in a single optomechanical system. It is found that the highest sensitivity for measuring the charges could be improved with more than four orders of magnitude in the presence of the assisted gain cavity than that in the absence of the assisted gain cavity.

II. THEORETICAL MODEL AND EQUATIONS

As shown in Fig. 1, the system is composed of two coupled cavities (denoted by cavity A and cavity B). The cavity A has cavity loss with loss rate κ_a and is made up of a fixed and a movable mirror with resonance frequency ω_c, where the movable one is treated as a charged mechanical resonator (MR) with resonance frequency ω_m, effective mass m, damping rate Γ_m, and charge Q_1. The cavity B is a gain cavity with resonance frequency ω_c and gain rate κ_b. Two cavities can couple by the photon hopping with strength J, which can be tuned by changing the distance between them. The cavity A is simultaneously driven by a strong pump field of frequency ω_1 with amplitude ε_1 and a weak probe field of frequency ω_p with amplitude ε_p. With the rotating-wave approximation of the system, the Hamiltonian of such a compound system can be written as [44–46]

$$\begin{aligned} H =& -\hbar\Delta(\hat{a}^\dagger\hat{a} + \hat{b}^\dagger\hat{b}) + \frac{\hat{p}^2}{2m} + \frac{1}{2}m\omega_m^2\hat{x}^2 + \hbar G\hat{x}\hat{a}^\dagger\hat{a} \\ &+ \hbar J(\hat{a}^\dagger\hat{b} + \hat{a}\hat{b}^\dagger) + i\hbar\sqrt{\eta_c\kappa_a}\varepsilon_1(\hat{a}^\dagger - \hat{a}) \\ &+ i\hbar\sqrt{\eta_c\kappa_a}(\hat{a}^\dagger e^{-i\Omega t}\varepsilon_p - \hat{a}e^{i\Omega t}\varepsilon_p^*) + \frac{kQ_1Q_2\hat{x}}{r^2}, \end{aligned} \tag{1}$$

where $\hat{a}$ and $\hat{b}$ ($\hat{a}^\dagger$ and $\hat{b}^\dagger$) are the annihilation (creation) operators of the loss and gain cavities, respectively. $\Delta = \omega_1 - \omega_c$ and $\Omega = \omega_p - \omega_1$ are the detunings of the loss cavity resonance frequency and the frequency of the probe laser from the pump laser, respectively. $\hat{p}$ ($\hat{x}$) is the momentum (position) operator of the MR. The first line describes the free Hamiltonian of the system. The parameter G is the optomechanical coupling constant. The term $i\hbar\sqrt{\eta_c\kappa_a}\varepsilon_1(\hat{a}^\dagger - \hat{a}) + i\hbar\sqrt{\eta_c\kappa_a}(\hat{a}^\dagger e^{-i\Omega t}\varepsilon_p - \hat{a}\, e^{i\Omega t}\varepsilon_p^*)$ describes the coupling between the two-tone input field and the loss cavity A. The coupling parameter η_c is chosen to be the critical coupling value 1/2 here and $\varepsilon_{p,1} = \sqrt{P_{p,1}/\hbar\omega_1}$ are the amplitudes of the input fields with the power $P_{p,1}$. The term $kQ_1Q_2\hat{x}/r^2$ describes the Coulomb interaction between the charged MR and the charged object with k the electrostatic force constant, r the distance between the MR and the charged object, and Q_1 and Q_2 the charge of the MR and the charged object, respectively. In order to study the charge-dependent effects of the optical second-order sideband (OSS), we fix the charge of the MR Q_1 and only focus on the case that $Q_2 = n\,e > 0$, with e the elementary charge and n the charge number in the present work.

In this work, we are interested in the mean response of the system, so the operators can be reduced to their expectation values, i.e., $a(t) \equiv \langle\hat{a}(t)\rangle$, $a^*(t) \equiv \langle\hat{a}^\dagger(t)\rangle$, $x(t) \equiv \langle\hat{x}(t)\rangle$, and $p(t) \equiv \langle\hat{p}(t)\rangle$. Taking the damping of two cavities and MR, the dynamics evolution of the system can be described by the following Heisenberg-Langevin equation [based on the Hamiltonian in Eq. (1)]:

$$\begin{aligned} \dot{a} =& \left(i\Delta - iGx - \frac{\kappa_a}{2}\right)a - iJb + \sqrt{\eta_c\kappa_a}\varepsilon_1 \\ &+ \sqrt{\eta_c\kappa_a}\varepsilon_p e^{-i\Omega t}, \end{aligned} \tag{2}$$

$$\dot{b} = \left(i\Delta - \frac{\kappa_b}{2}\right)b - iJa, \tag{3}$$

$$\dot{x} = p/m, \tag{4}$$

$$\dot{p} = -m\omega_m^2 x - \hbar G a^\dagger a - \Gamma_m p - \frac{kQ_1Q_2}{r^2}, \tag{5}$$

where Γ_m is the decay rate of the MR. The mean-field approximation by factorizing averages has been used, and the quantum noise terms are neglected safely in the semiclassical approximation, which is demonstrated to be valid in the concerned weak-coupling regime [26]. As the pump field ε_1 is much stronger than the probe field ε_p, we can obtain the steady-state solution of Eqs. (2)–(5) by means of the perturbation method. To this end, the total solution of Eqs. (2)–(5) can be described by $o = o_s + \delta o$ ($o = a, a^\dagger, b, b^\dagger, x, p$), where o_s

are the steady-state solutions merely associated with the pump field. The steady-state solution can be obtained as

$$a_s = -\frac{\sqrt{\eta_c\kappa_a}\varepsilon_1}{\left(i\Delta - iGx_s - \frac{\kappa_a}{2}\right) + \frac{J^2}{i\Delta - \frac{\kappa_b}{2}}}, \tag{6}$$

$$b_s = \frac{iJ}{i\Delta - \frac{\kappa_b}{2}}a_s, \tag{7}$$

$$x_s = \frac{-\hbar G|a_s|^2 - \xi Q_2}{m\omega_m^2}, \tag{8}$$

where $\xi = kQ_1/r^2$. We now turn to consider the perturbation made by the probe field. The evolution of the perturbation terms δa, δb, δp, and δx caused by the probe field can be written as

$$\dot{\delta a} = \left(i\Delta - iGx_s - \frac{\kappa_a}{2}\right)\delta a - iJ\delta b - iGa_s\delta x - iG\delta a\delta x + \sqrt{\eta_c\kappa_a}\varepsilon_p e^{-i\Omega t}, \tag{9}$$

$$\dot{\delta b} = \left(i\Delta - \frac{\kappa_b}{2}\right)\delta b - iJ\delta a, \tag{10}$$

$$\dot{\delta x} = \frac{\delta p}{m}, \tag{11}$$

$$\dot{\delta p} = -m\omega_m^2\delta x - \hbar G(a_s\delta a^* + a_s^*\delta a) - \Gamma_m\delta p - \hbar G\delta a^*\delta a. \tag{12}$$

We then assume that the solutions of Eqs. (9)–(12) have the following forms:

$$\delta a = A_1^- e^{-i\Omega t} + A_1^+ e^{i\Omega t} + A_2^- e^{-2i\Omega t} + A_2^+ e^{2i\Omega t}, \tag{13}$$

$$\delta a^* = (A_1^-)^* e^{i\Omega t} + (A_1^+)^* e^{-i\Omega t} + (A_2^-)^* e^{2i\Omega t} + (A_2^+)e^{-2i\Omega t}, \tag{14}$$

$$\delta b = B_1^- e^{-i\Omega t} + B_1^+ e^{i\Omega t} + B_2^- e^{-2i\Omega t} + B_2^+ e^{2i\Omega t}, \tag{15}$$

$$\delta b^* = (B_1^-)^* e^{i\Omega t} + (B_1^+)^* e^{-i\Omega t} + (B_2^-)^* e^{2i\Omega t} + (B_2^+)^* e^{-2i\Omega t}, \tag{16}$$

$$\delta x = X_1 e^{-i\Omega t} + X_1^* e^{i\Omega t} + X_2 e^{-2i\Omega t} + X_2^* e^{2i\Omega t}, \tag{17}$$

where the coefficient $A_1^{\mp}$ ($A_2^{\mp}$) is the coefficient of the first- (second-) order sideband with frequency $\omega_1 \pm \Omega$ ($\omega_1 \pm 2\Omega$), with the signs $+$ and $-$ in $A_1^{\mp}$ ($A_2^{\mp}$) corresponding to the lower and upper sidebands, respectively. By substituting Eqs. (13)–(17) into Eqs. (9)–(12) and comparing the coefficients of the same order, we can obtain the amplitude of the first-order sideband and OSS (the detailed derivation is shown in the Appendix):

$$A_1^- = \frac{[1+if(\Omega)]\sqrt{\eta_c\kappa_a}\varepsilon_p}{\left[\frac{\kappa_a}{2} - i(\Delta+\Omega)\right][1+if(\Omega)] - i\hbar G^2\chi(\Omega)|a_s|^2 + f_1(\Omega)}, \tag{18}$$

$$A_2^- = \frac{M_0(\Omega, Q_2)A_1^- X_1 + M_3(\Omega, Q_2)X_1^2}{M_4(\Omega, Q_2)M_5(\Omega, Q_2) - M_6(\Omega, Q_2)}, \tag{19}$$

where $X_1 = -\hbar G\chi(\Omega)a_s A_1^-/[1+if(\Omega)]$, $f(\Omega) = \hbar G^2\chi(\Omega)|a_s|^2/\{[\kappa_a/2 + i(\bar{\Delta} - \Omega)] + J^2/[\kappa_b/2 + i(\Delta - \Omega)]\}$, $f_1(\Omega) = [1 + if(\Omega)]J^2/[\kappa_b/2 + i(\Delta - \Omega)]$, $\bar{\Delta} = \Delta - Gx_s$, $M_0(\Omega, Q_2) = M_2(\Omega, Q_2) - \frac{1}{2}iGM_1(\Omega, Q_2)$, $M_1(\Omega, Q_2) = 2\Theta(Q_2) - 4i\Omega + 2\alpha_2(\Omega) + 2i\hbar G^2|a_s|^2\chi_1(\Omega)$, $M_2(\Omega, Q_2) = -\hbar G^3|a_s|^2\chi_1(\Omega)[2\Theta(Q_2) - 4i\Omega + 2\alpha_2(\Omega)]/[2\Theta(Q_2) - 2i\Omega + 2\alpha_3(\Omega)]$, $M_3(\Omega, Q_2) = -2\hbar G^3|a_s|^2 a_s\chi_1(\Omega)/[2\Theta(Q_2) - 2i\Omega + 2\alpha_3(\Omega)]$, $M_4(\Omega, Q_2) = \Theta(Q_2) - 2i\Omega + \alpha_1(\Omega)$, $M_5(\Omega, Q_2) = \Theta(Q_2) - 2i\Omega + \alpha_2(\Omega) + i\hbar G^2|a_s|^2\chi_1(\Omega)$, $M_6(\Omega, Q_2) = i\hbar G^2|a_s|^2\chi_1(\Omega)[\Theta(Q_2) - 2i\Omega + \alpha_2(\Omega)]$, $\Theta(Q_2) = i\Delta + \frac{\kappa_a}{2} + (i\hbar G^2|a_s|^2 + iG\xi Q_2)/m\omega_m^2$, $\alpha_1(\Omega) = J^2/[(\kappa_b/2) - i(\Delta + 2\Omega)]$, $\alpha_2(\Omega) = J^2/[(\kappa_b/2) + i(\Delta - 2\Omega)]$, $\alpha_3(\Omega) = J^2/[(\kappa_b/2) + i(\Delta - \Omega)]$, $\chi(\Omega) = 1/m(\omega_m^2 - \Omega^2 - i\Gamma_m\Omega)$, and $\chi_1(\Omega) = 1/m(\omega_m^2 - 4\Omega^2 - 2i\Gamma_m\Omega)$.

According to the input-output relation of the cavity $s_{\text{out}} = s_{\text{in}} - \sqrt{\eta_c\kappa_a}a$ [21], we can obtain the output field as follows:

$$s_{\text{out}} = c_1 e^{-i\omega_1 t} + c_p e^{-i\omega_p t} - \sqrt{\eta_c\kappa_a}A_2^- e^{-i(2\omega_p - \omega_1)t} - \sqrt{\eta_c\kappa_a}A_1^+ e^{-i(2\omega_1 - \omega_p)t} - \sqrt{\eta_c\kappa_a}A_2^+ e^{-i(3\omega_1 - 2\omega_p)}, \tag{20}$$

where $c_1 = \varepsilon_1 - \sqrt{\eta_c\kappa_a}a_s$ and $c_p = \varepsilon_p - \sqrt{\eta_c\kappa_a}A_1^-$. The terms $c_1 e^{-i\omega_1 t}$ and $c_p e^{-i\omega_p t}$ denote the output signals corresponding to the frequency of ω_1 and ω_p, respectively. The transmission of the probe field can be defined as $t_p = c_p/\varepsilon_p$, with the optical transmission strength

$$|t_p|^2 = \left|1 - \frac{\sqrt{\eta_c\kappa_a}A_1^-}{\varepsilon_p}\right|^2. \tag{21}$$

The term $-\sqrt{\eta_c\kappa_a}A_1^+ e^{-i(2\omega_1 - \omega_p)t}$ represents the Stokes process. The term $-\sqrt{\eta_c\kappa_a}A_2^- e^{-i(2\omega_p - \omega_1)t}$ describes the upper OSS process, in which the output field with frequency $\omega_1 + 2\Omega$ can be produced, while the term $-\sqrt{\eta_c\kappa_a}A_2^+ e^{-i(3\omega_1 - 2\omega_p)t}$ describes the lower OSS process, in which the output field with frequency $\omega_1 - 2\Omega$ can be produced. We should note that here we focus on the process of the upper OSS in the present system. To this end, we introduce the dimensionless quantity

$$\eta = \left|-\frac{\sqrt{\eta_c\kappa_a}A_2^-}{\varepsilon_p}\right| \tag{22}$$

for describing the efficiency of the upper OSS process.

III. ENHANCED GENERATION OF OPTICAL SECOND-ORDER SIDEBAND

In this section, we analyze the creation and enhancement of the charge-dependent effect of the optical second-order sideband (OSS) in the present hybrid optomechanical system. As mentioned above, the coupling parameter J between gain and loss cavities can be adjusted efficiently. In the cases of $J = 0$, the hybrid optomechanical system could degenerate into a cavity optomechanical system in the presence of the Coulomb interaction. From Eqs. (21) and (22), one finds that the transmission $|t_p|^2$ and the OSS efficiency η depend on the coupling parameter J and the charge Q_2 of the object.

In order to examine how an assisted gain cavity (cavity B) coupling to the cavity A modifies the transmission of the probe field and OSS process, we first provide in Figs. 2(a) and 2(b) the comparative results of the transmission and the OSS spectrum without including the charged object ($Q_2 = 0$) for

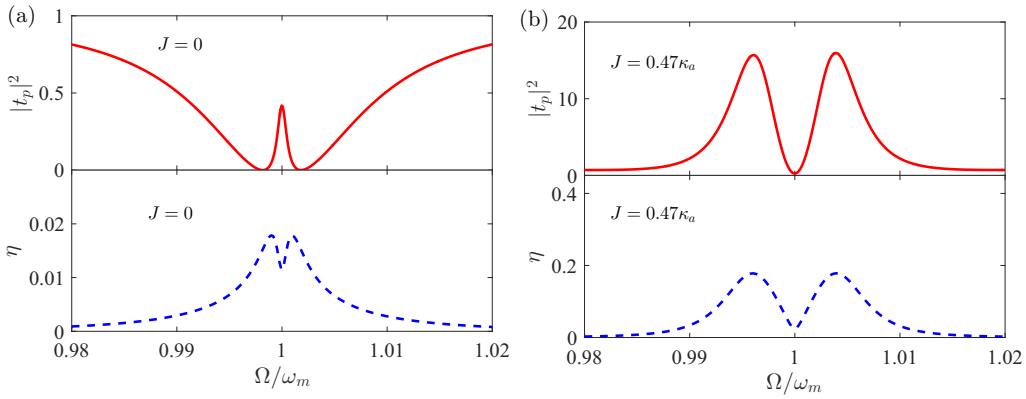

FIG. 2. Simulation results of the transmission intensity of probe field $|t_p|^2$ and the efficiency of second-order upper sideband η as a function of the detuning Ω/ω_m for two different arrangements of the hybrid optomechanical system: (i) a single lossy cavity optomechanical system ($J = 0$) [panels (a)] and (ii) a gain-cavity-assisted optomechanical (GCAOM) system with the coupling strength $J = 0.47\kappa_a$ [panels (b)]. The other parameters are $\Delta = -\omega_m$, $m = 20$ ng, $\omega_m = 2\pi \times 52.8$ MHz, $\Gamma_m = 2\pi \times 40$ kHz, $G = -2\pi \times 12$ GHz/nm, $\kappa_a = 2\pi \times 2$ MHz, $\kappa_b = -\kappa_a$, $r = 67$ μm, $Q_1 = CU$ with $C = 27.5$ nF (C is the capacitance of a capacitor) and $U = 1$ V, and $\eta_c = 0.5$. The wavelength of the pump field $\lambda = 532$ nm and the value of the powers of the driven field and the probe field are as follows: $P_1 = 210.3$ μW and $\varepsilon_p = 0.05\varepsilon_1$.

two different cases, i.e., a single loss cavity optomechanical system ($J = 0$) and a cavity optomechanical system assisted by a gain cavity ($J = 0.47\kappa_a$), respectively. In the absence of the gain cavity ($J = 0$), one can find from Fig. 2(a) that the curve of $|t_p|^2$ exhibits a conventional OMIT profile with a low transmission peak located at $\Omega = \omega_m$ and two deep absorbed valleys located at $\Omega \approx 0.999\omega_m$ and $\Omega \approx 1.001\omega_m$. Correspondingly, the spectrum of the OSS η shown in Fig. 2(a) exhibits a shallow valley and two symmetric peaks with low peak value ($\eta_{\max} < 0.02$). The shallow valley locates at the position of the resonance frequency $\Omega = \omega_m$, which means that the OSS process is suppressed when the transmission of the probe field occurs. This phenomena shown in Fig. 2(a) is consistent with that shown in Ref. [47]. In contrast to the conventional OMIT profile in a lossy cavity optomechanical system, it can be seen from Fig. 2(b) that an inverted-OMIT profile [48,49] of the transmission spectrum occurs when a gain cavity is included, characterizing an absorbed valley between two symmetric strongly amplifying peaks. This can be intuitively explained as follows. Under the assistance of the gain cavity, the absorbed valleys due to the lossy cavity were filled and transformed into amplifying peaks, indicating that the input field is efficiently amplified and hence the optical transmission intensity $|t_p|^2$ is amplified [50]. Simultaneously, an absorbed valley was induced by the gain cavity in the spectral region where otherwise strong amplification occurs to produce inverted OMIT. Furthermore, one can find that the spectrum of η also exhibits two peaks ($\eta_{\max} \sim 0.2$) when the gain cavity is included, which indicates that amplification of the transmission leads to the enhanced up-converted process (i.e., the increasing of η). Direct comparison of the peaks of η for two cases $J = 0$ and $J = 0.47\kappa_a$ implies that an assisted gain cavity provides more than one order of enhancement for the OSS generation.

Considering the coupling between the optomechanical system and the charged object (i.e., $Q_2 \neq 0$), the contour map of the efficiency η as the function of both n and the detuning Ω/ω_m is displayed in Fig. 3. The maps of Figs. 3(a) and 3(b), respectively, correspond to two cases of $J = 0$ (without the assisted gain cavity) and $J = 0.47\kappa_a$ (with the assisted gain cavity). In the absence of the assisted gain cavity ($J = 0$), Fig. 3(a) shows that the peak value of OSS η does not depend significantly on the number of the charges n. However, in the presence of the gain cavity ($J = 0.47\kappa_a$), Fig. 3(b) shows that the peak value of the OSS η increases almost linearly as the increase of the charge numbers n. It can be also seen from Fig. 3(b) that the maximal values of the OSS η are 0.18 and 0.46 corresponding to the charge numbers $n = 0$ and $n = 8$, respectively. In other words, the maximal OSS efficiency $\eta_{\max}$ is enhanced by the Coulomb interaction for more than 20%. Thus we can conclude that an assisted gain cavity can amplify the charge-dependent effect of the OSS efficiency. In addition, the OSS spectra shown in Fig. 3 becomes asymmetric as the charge number n increases. This asymmetry of the OSS spectra might arise from the varying of the equilibrium position of the MR and the modification of spring constant due to the enhanced Coulomb interaction. As a matter of fact, the change of the MR position will result in the shift of the lossy optical resonant frequency, making it detuned from the assisted gain cavity. Because the optical pump frequency is always fixed, as the charge number is increased, the pump is more and more "off-detuned." As a result, the center valley and peaks of the OSS spectra in Fig. 3 shift toward one side and the spectra of η exhibits asymmetry.

In order to provide direct insight into the role of the gain cavity on the OSS generation, the maximal value of the efficiency $\eta_{\max}$ versus J is depicted in Fig. 4(a). One can find from Fig. 4(a) that the maximal efficiency $\eta_{\max}$ remains unchanged with the increase of J first when $J < 0.24\kappa_a$, then goes through exponential growth as the value of J increases when $J > 0.24\kappa_a$. It should be noted that the pump field has been widely used for modulation of the optical nonlinearity in the field of cavity quantum electrodynamics [51–57]. According to Eq. (22), the OSS efficiency η depends on the input power of the pump field. In order to explicitly show the influence of the pump field on the generated OSS

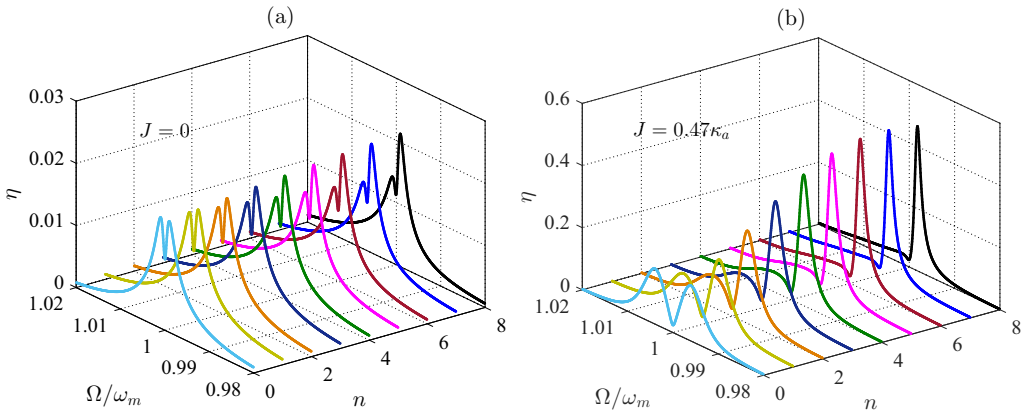

FIG. 3. Simulation results of the efficiency η of optical second-order upper sideband generation as a function of the detuning Ω/ω_m and the charge number n for two different arrangements of the hybrid optomechanical system: (a) a single lossy cavity optomechanical system ($J = 0$) and (b) a gain-cavity-assisted optomechanical (GCAOM) system with the coupling strength $J = 0.47\kappa_a$. The other system parameters are exactly the same as in Fig. 2.

spectra with fixed coupling strength $J = 0.47\kappa_a$, we show in Fig. 4(b) the peak value $\eta_{\max}$ of the OSS versus the power P_1 for several different charge numbers n. It can be found from this figure that $\eta_{\max}$ increases as P_1 increases first, and then decreases slightly because of the saturation of the MR. With the further increase of the pump power to a higher value, a steady-state regime is reached, with MR proceeding at a fixed amplitude. These are so-called self-induced (backaction-induced) optomechanical oscillations [26]. As a matter of fact, they are analogous to the lasing action, but now in a mechanical system and with the incoming laser radiation providing the pump. According to Eqs. (2)–(5), the bias gate voltage U of MR can be used to modulate this Coulomb interaction. By fixing the pump power ($P_1 = 210.3\ \mu$W) and the coupling strength $J = 0.47\kappa_a$, we show in Fig. 4(c) the maximal OSS efficiency $\eta_{\max}$ versus the bias gate voltage U for different charge numbers n. Within a reasonable range of voltage, one can find that $\eta_{\max}$ increases monotonically with the increase of the bias gate voltage U for all n, which confirmed that the stronger Coulomb interaction leads to more pronounced OSS generation. In addition, Fig. 4 also shows that the increase of $\eta_{\max}$ has a strong dependence on the charge number of the charged object, which is in agreement with the above results in Fig. 3. This dependence becomes more pronounced as the values of parameters (J, P_1, and U) increase.

IV. HIGH-SENSITIVITY CHARGE SENSORS BASED ON THE SPECTRA OF SECOND-ORDER SIDEBAND

It has been shown in Figs. 2–4 that the Coulomb interaction had profound effects on the amplifying optical second-order sideband (OSS) in a gain-cavity-assisted optomechanical system. In other words, the change of charge number n of a charged object can shift the equilibrium position of the mechanical resonator and then modify the amplitude of OSS. Such a charge-dependent effect of OSS is well suited for application in a high-sensitivity sensor. Subsequently we discuss the application of such a gain-cavity-assisted optomechanical system as a family of high-sensitivity sensors for measuring the charges. Here, a practical setup for heterodyne frequency-beat measurement of OSS is briefly shown in Fig. 5. The working scheme is initially set up by inputting a continuous-wave pump laser ω_1 with a fixed wavelength and input power. The output of the pump laser is divided into two beams in beam splitter BS1. The transmitting beam is frequency shifted

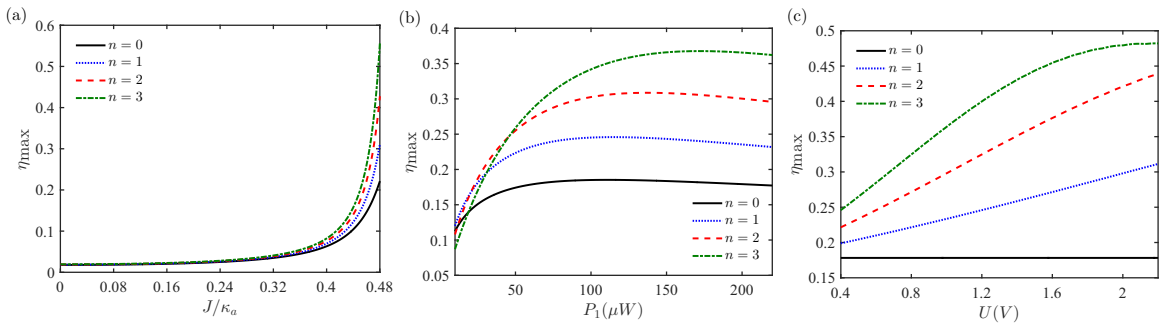

FIG. 4. Simulation results of the maximal efficiency $\eta_{\max}$ vs (a) the coupling strength J between the loss and gain cavity with $P_1 = 210.3\ \mu$W and $U = 1$ V, (b) the power of pump field P_1 with $J = 0.47\kappa_a$ and $U = 1$ V, and (c) the bias gate voltage U with $J = 0.47\kappa_a$ and $P_1 = 210.3\ \mu$W, for different charge number n. The solid, dotted, dashed, and dash-dotted lines, respectively, correspond to the different charge numbers $n = 0$, $n = 1$, $n = 2$, and $n = 3$. The other parameters are exactly the same as in Fig. 2(b).

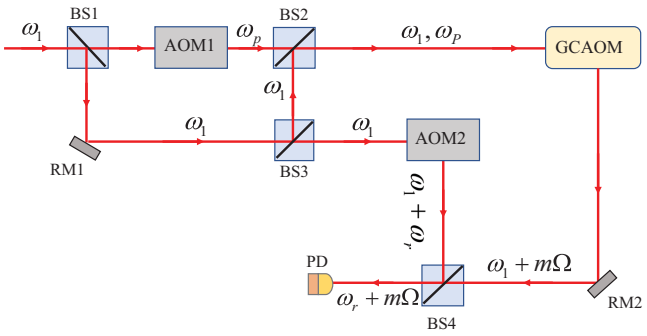

FIG. 5. Schematic diagram of the setup for heterodyne frequency-beat measurement of optical second-order sideband (OSS). BS, beam splitter; AOM, acousto-optic modulator; GCAOM, gain-cavity-assisted optomechanical system; RM, reflected mirror; PD, photodetector. ω_l indicates the frequency of the input pump laser, ω_p is the frequency of the probe beam, and ω_r is the frequency of the reference beam.

by an acousto-optic modulator (AOM1) as a probe beam (ω_p). The reflected beam (ω_l) is reflected by a reflected mirror (RM) and then divided into two beams in beam splitter BS3. The reflected beam of BS3 is mixed with the transmitting beam in beam splitter BS2. The mixed beam of the probe and pump laser with two-frequency components (ω_l and ω_p) then is injected into the gain-cavity-assisted optomechanical (GCAOM) system and generates the higher-order sidebands. The transmitting beam of BS3 is frequency shifted by another acousto-optic modulator (AOM2) with shifted frequency ω_r. Finally, the output beams of the GCAOM with frequency components (ω_l) and higher-order sidebands ($m\Omega$) are mixed with the output beams of AOM2 for heterodyne frequency-beat measurement. The beat note between the beams transmitted through the GCAOM and the AOM2 path was then detected using a fast photodetector and visualized using a radio-frequency spectrum analyzer. The OSS and high-order sidebands are resolved by using heterodyne frequency-beat measurement even though the frequency difference between the different frequency components is $2\pi \times 80$ MHz (i.e., $\Omega = 2\pi \times 80$ MHz) [58].

For the optical second-order sideband (OSS), the sensitivity to the charge-induced shift of the maximal OSS $\eta_{\max}$ is defined as

$$S \equiv \left| \frac{\Delta\eta_{\max}}{\Delta n} \right|. \tag{23}$$

Based on Eq. (23), we can calculate the sensitivity S to show the difference for two different arrangements of the hybrid optomechanical system: $S = 4.9 \times 10^{-4}$ for a single lossy cavity optomechanical system ($J = 0$); $S = 5.8 \times 10^{-2}$ for a gain-cavity-assisted optomechanical system with the fixed coupling strength $J = 0.47\kappa_a$. Obviously, an assisted gain cavity can significantly enhance the sensitivity of the charge detection.

As illustrated in Fig. 4, charge-induced shift of the maximal efficiency $\Delta\eta_{\max}$ depends on the parameters of the present system, such as coupling strength between the loss and gain cavity (J), the power of the pump field (P_l), and the bias gate voltage of the charged body U. In order to further verify the influence of these parameters on modifying the sensitivity, we show in the insets of Fig. 6 the peak value of the OSS $\eta_{\max}$ versus the charge number n for several different values of these parameters (J, P_l, and U). It can be seen from the inset of Fig. 6(a) increasing J provides a notable enhancement of $\eta_{\max}$ for all n and the slope (the sensitivity S) of the fitting curve increases as the increase of J. Figure 6(a) shows that the sensitivity S grows exponentially with the increase of J. The sensitivity S can be modulated by the pump power P_l. In the inset of Fig. 6(b), we show $\eta_{\max}$ versus the charge number n at several different values of pump power P_l ranging from 50.3 μW to 210.3 μW for a given coupling parameter $J = 0.47\kappa_a$. Obviously, the slope of the fitting curve increases with the increase of the power of pump field P_l. In other words, the sensitivity can be improved via increasing pump power, as illustrated in Fig. 6(b). In the inset of Fig. 6(c), we present the peak value $\eta_{\max}$ of OSS as a function of the charge number n for several different bias gate voltage U ranging from 0.1 V to 1.5 V. It can be found that the slope of the fitting curve increases as the

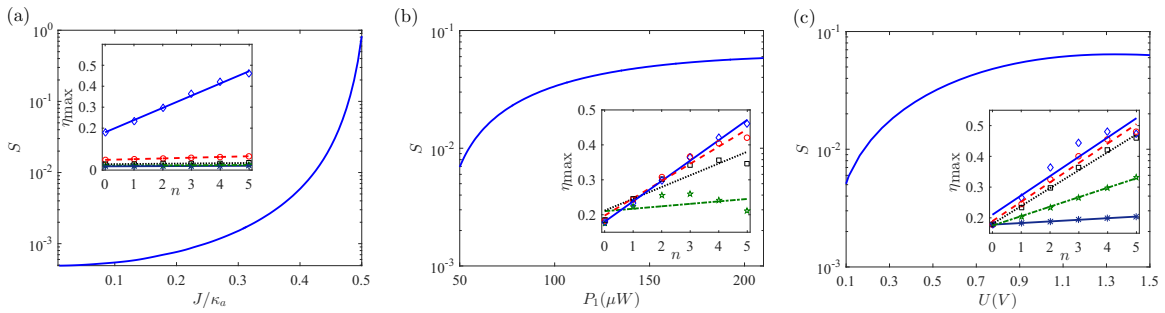

FIG. 6. Simulation results of the sensitivity S vs (a) coupling parameters J, (b) the power P_l of the pump field, and (c) the bias gate voltage U of the charge body. Inset: simulation results of the peak value $\eta_{\max}$ as a function of charge number n for different coupling parameters J in panel (a), i.e., $J = 0$ (smalt, asterisk), $J = 0.17\kappa_a$ (green, pentagon), $J = 0.27\kappa_a$ (black, square), $J = 0.37\kappa_a$ (red, circle), and $J = 0.47\kappa_a$ (blue, diamond), different power P_l of the pump field in panel (b), i.e., $P_l = 50.3$ μW (green, pentagon), $P_l = 100.3$ μW (black, square), $P_l = 150.3$ μW (red, circle), and $P_l = 210.3$ μW (blue, diamond), (c) different bias gate voltage U of the charge body in panel (c), i.e., $U = 0.1$ V (smalt, asterisk), $U = 0.5$ V (green, pentagon), $U = 1$ V (black, square), $U = 1.2$ V (red, circle), and $U = 1.5$ V (blue, diamond). The other parameters are exactly the same as in Fig. 4.

increase of the bias gate voltage. Correspondingly, as shown in Fig. 6(c), the sensitivity S increases slowly from a small value with increasing of the bias gate voltage. From what has been analyzed above, we can reach the conclusion that, with proper choice of P_1 and U, a improved sensitivity for charge detection can be realized in the present gain-cavity-assisted optomechanical system.

V. CONCLUSIONS

In conclusion, we have theoretically investigated the enhanced charge-dependent generation of the optical second-order sidebands (OSS) in a gain-cavity-assisted optomechanical system coupled to a charged object. Beyond the conventional linearized description of optomechanical interactions, the nonlinear interaction between the cavity field and the mechanical oscillation in a gain-cavity-assisted optomechanical system coupled to a charged object are included in the Heisenberg-Langevin equations. The analytical expression describing and featuring the charge-dependent generation of the OSS is obtained by means of the perturbation method. Our results showed that an assisted gain cavity can significantly enhance the generation of the OSS, and can also lead to higher charge dependence of the OSS spectrum than that achieved from a single optomechanical system coupled to a charged object. The present investigations may lead to better understanding of the crossover between nonlinear spectroscopy and Coulomb interaction in hybrid electro-optomechanical systems.

More importantly, the highly sensitive charge-dependent effects of the OSS can be used to devise a type of high-sensitivity optical sensor for measuring the charges. We analyze the influences of the coupling strength J between the loss and gain cavities, the power of the pump field P_1, and the bias gate voltage of the charged MR U on the sensitivity of the sensor. The present results showed the sensitivity grows exponentially with the increase of the coupling strength J. For achievable parameters in practical experiments, the sensitivity for the gain-cavity-assisted optomechanical system is more than 10^4 higher than that in a single lossy optomechanical system. In addition, the sensitivity of the sensor also increases as the power P_1 of the pump field and the bias gate voltage U of the charged MR increase. We believe that the proposed structure is feasible in experimental realizations and deserves to be tested under the currently existing experimental conditions [59]. The present investigation provides a route toward modulating the nonlinear optical properties of the electro-optic hybrid system, as well as guiding the design of sensitive devices.

ACKNOWLEDGMENTS

The research is supported in part by National Natural Science Foundation of China under Grants No. 11774054 and No. 11775190 and by Natural Science Foundation of Jiangsu Province under Grant No. BK20161410.

APPENDIX: DERIVING THE COEFFICIENT OF THE FIRST- (SECOND-) ORDER SIDEBAND

In order to obtain the amplitudes of the upper first-order sideband and the upper second-order sideband, we substitute Eqs. (13)–(17) into Eqs. (9)–(12); then we obtain some equations about the coefficient $A_1^{\pm}$ and $A_2^{\pm}$ as follows:

$$-i\Omega A_1^- = \left(i\Delta - iGx_s - \frac{\kappa_a}{2}\right)A_1^- - iJB_1^- - iGa_sX_1 - iG(A_1^+X_2 + A_2^-X_1^*) + \sqrt{\eta_c\kappa_a}\varepsilon_p, \tag{A1}$$

$$i\Omega A_1^+ = \left(i\Delta - iGx_s - \frac{\kappa_a}{2}\right)A_1^+ - iJB_1^+ - iGa_sX_1^* - iG(A_1^-X_2^+ + A_2^+X_1), \tag{A2}$$

$$-2i\Omega A_2^- = \left(i\Delta - iGx_s - \frac{\kappa_a}{2}\right)A_2^- - iJB_2^- - iGa_sX_2 - iGA_1^-X_1, \tag{A3}$$

$$2i\Omega A_2^+ = \left(i\Delta - iGx_s - \frac{\kappa_a}{2}\right)A_2^+ - iJB_2^+ - iGa_sX_2^* - iGA_1^+X_1^*, \tag{A4}$$

where $X_1 = -\hbar\chi G[a_s(A_1^+)^* + a_s^*A_1^-]$, $\chi = 1/m(\omega_m^2 - \Omega^2 - i\Gamma_m\Omega)$, $X_2 = -\hbar\chi_1 G[a_s(A_2^+)^* + a_s^*A_2^- - A_1^-(A_1^+)^*]$, $\chi_1 = 1/m(\omega_m^2 - 4\Omega^2 - 2i\Gamma_m\Omega)$, $B_1^- = \frac{-iJA_1^-}{\frac{\kappa_b}{2} - i(\Delta+\Omega)}$, $B_1^+ = \frac{-iJA_1^+}{\frac{\kappa_b}{2} - i(\Delta-\Omega)}$, $B_1^- = \frac{-iJA_2^-}{\frac{\kappa_b}{2} - i(\Delta+2\Omega)}$, and $B_2^+ = \frac{-iJA_2^+}{\frac{\kappa_b}{2} - i(\Delta-2\Omega)}$. By solving Eqs. (A1)–(A4), we can obtain the amplitudes of the upper first-order sideband and the upper second-order sideband as shown in Eq. (18) and Eq. (19).

[1] C. M. Caves, Quantum-Mechanical Radiation-Pressure Fluctuations in an Interferometer, Phys. Rev. Lett. **45**, 75 (1980).

[2] S. Chu, L. Hollberg, J. E. Bjorkholm, A. Cable, and A. Ashkin, Three-Dimensional Viscous Confinement and Cooling of Atoms by Resonance Radiation Pressure, Phys. Rev. Lett. **55**, 48 (1985).

[3] S. Huang, and G. S. Agarwal, Normal-mode splitting and antibunching in Stokes and anti-Stokes processes in cavity optomechanics: Radiation-pressure-induced four-wave-mixing cavity optomechanics, Phys. Rev. A **81**, 033830 (2010).

[4] S. Huang, and G. S. Agarwal, Electromagnetically induced transparency with quantized fields in optocavity mechanics, Phys. Rev. A **83**, 043826 (2011).

[5] Z. Wu, R. H. Luo, J. Q. Zhang, Y. H. Wang, W. Yang, and M. Feng, Force-induced transparency and conversion between slow and fast light in optomechanics, Phys. Rev. A **96**, 033832 (2017).

[6] Q. C. Liu, T. F. Li, X. Q. Luo, H. Zhao, W. Xiong, Y. S. Zhang, Z. Chen, J. S. Liu, W. Chen, F. Nori, J. S. Tsai, and J. Q. You, Method for identifying electromagnetically induced transparency in a tunable circuit quantum electrodynamics system, Phys. Rev. A **93**, 053838 (2016).

[7] E. Verhagen, S. Deléglise, S. Weis, A. Schliesser, and T. J. Kippenberg, Quantum-coherent coupling of a mechanical oscillator to an optical cavity mode, Nature (London) **482**, 63 (2012).

[8] D. E. Chang, A. H. Safavi-Naeini, M. Hafezi, and O. Painter, Slowing and stopping light using an optomechanical crystal array, New J. Phys. **13**, 023003 (2011).

[9] O. Arcizet, P. F. Cohadon, T. Briant, M. Pinard and A. Heidmann, Radiation-pressure cooling and optomechanical instability of a micromirror, Nature (London) **444**, 71 (2006).

[10] J. M. Dobrindt, I. Wilson-Rae, and T. J. Kippenberg, Parametric Normal-Mode Splitting in Cavity Optomechanics, Phys. Rev. Lett. **101**, 263602 (2008).

[11] S. Gröblacher, K. Hammerer, M. R. Vanner, and M. Aspelmeyer, Observation of strong coupling between a micromechanical resonator and an optical cavity field, Nature (London) **460**, 724 (2009).

[12] P. C. Ma, J. Q. Zhang, Y. Xiao, M. Feng, and Z. M. Zhang, Tunable double optomechanically induced transparency in an optomechanical system, Phys. Rev. A **90**, 043825 (2014).

[13] E. Gavartin, P. Verlot, and T. J. Kippenberg, A hybrid on-chip optomechanical transducer for ultrasensitive force measurements, Nat. Nanotechnol. **7**, 509 (2012).

[14] A. G. Krause, M. Winger, T. D. Blasius, Q. Lin, and O. Painter, A high-resolution microchip optomechanical accelerometer, Nat. Photon. **6**, 768 (2012).

[15] Y.-L. Chen, W.-L. Jin, Y.-F. Xiao, and X. Zhang, Measuring the Charge of a Single Dielectric Nanoparticle Using a High-Q Optical Microresonator, Phys. Rev. Appl. **6**, 044021 (2016).

[16] X. F. Liu, Y. Li, and H. Jing, Casimir switch: steering optical transparency with vacuum forces, Sci. Rep. **6**, 27102 (2016).

[17] Q. Wang, J. Q. Zhang, P. C. Ma, C. M. Yao, and M. Feng, Precision measurement of the environmental temperature by tunable double optomechanically induced transparency with a squeezed field, Phys. Rev. A **91**, 063827 (2015).

[18] W. J. Nie, A. X. Chen, and Y. H. Lan, Coupling mechanical motion of a single atom to a micromechanical cantilever, Opt. Exp. **25**, 32931 (2017).

[19] G. S. Agarwal and S. Huang, Optomechanical systems as single-photon routers, Phys. Rev. A **85**, 021801 (2012).

[20] P. Rabl, Photon Blockade Effect in Optomechanical Systems, Phys. Rev. Lett. **107**, 063601 (2011).

[21] S. Weis, R. Rivière, S. Deléglise, E. Gavartin, O. Arcizet, A. Schliesser, and T. J. Kippenberg, Optomechanically induced transparency, Science **330**, 1520 (2010).

[22] A. H. Safavi-Naeini, T. P. Mayer Alegre, J. Chan, M. Eichenfield, M. Winger, Q. Lin, J. T. Hill, D. E. Chang, and O. Painter, Electromagnetically induced transparency and slow light with optomechanics, Nature (London) **472**, 69 (2011).

[23] M. Fleischhauer, A. Imamoglu, and J. P. Marangos, Electromagnetically induced transparency: Optics in coherent media, Rev. Mod. Phys. **77**, 633 (2005).

[24] J.-Q. Zhang, Y. Li, M. Feng, and Y. Xu, Precision measurement of electrical charge with optomechanically induced transparency, Phys. Rev. A **86**, 053806 (2012).

[25] H. Xiong, Z. X. Liu, and Y. Wu, Highly sensitive optical sensor for precision measurement of electrical charges based on optomechanically induced difference-sideband generation, Opt. Lett. **42**, 3630 (2017).

[26] M. Aspelmeyer, T. J. Kippenberg, and F. Marquardt, Cavity optomechanics, Rev. Mod. Phys. **86**, 1391 (2014).

[27] G. S. Agarwal, and S. Huang, Electromagnetically induced transparency in mechanical effects of light, Phys. Rev. A **81**, 041803 (2010).

[28] A. Kronwald and F. Marquardt, Optomechanically Induced Transparency in the Nonlinear Quantum Regime, Phys. Rev. Lett. **111**, 133601 (2013).

[29] W. X. Yang, A. X. Chen, X. T. Xie, and L. Ni, Enhanced generation of higher-order sidebands in a single-quantum-dot-cavity system coupled to a PT-symmetric double cavity, Phys. Rev. A **96**, 013802 (2017).

[30] H. Xiong, L. G. Si, X. Y. Lü, X. Yang, and Y. Wu, Carrier-envelope phase-dependent effect of high-order sideband generation in ultrafast driven optomechanical system, Opt. Lett. **38**, 353 (2013).

[31] H. Suzuki, E. Brown, and R. Sterling, Nonlinear dynamics of an optomechanical system with a coherent mechanical pump: Second-order sideband generation, Phys. Rev. A **92**, 033823 (2015).

[32] P. DelHaye, A. Schliesser, O. Arcizet, T. Wilken, R. Holzwarth, and T. J. Kippenberg, Optical frequency comb generation from a monolithic microresonator, Nature (London) **450**, 1214 (2007).

[33] Z. H. Musslimani, K. G. Makris, R. El-Ganainy, and D. N. Christodoulides, Optical Solitons in PT Periodic Potentials, Phys. Rev. Lett. **100**, 030402 (2008).

[34] H. Xiong, J. Gan, and Y. Wu, Kuznetsov-Ma Soliton Dynamics Based on the Mechanical Effect of Light, Phys. Rev. Lett. **119**, 153901 (2017).

[35] X. Y. Lü, H. Jing, J. Y. Ma, and Y. Wu, $\mathcal{PT}$-Symmetry-Breaking Chaos in Optomechanics, Phys. Rev. Lett. **114**, 253601 (2015).

[36] J. Li, J. Li, Q. Xiao, and Y. Wu, Giant enhancement of optical high-order sideband generation and their control in a dimer of two cavities with gain and loss, Phys. Rev. A **93**, 063814 (2016).

[37] C. Kong, H. Xiong, and Y. Wu, Coulomb-interaction-dependent effect of high-order sideband generation in an optomechanical system, Phys. Rev. A **95**, 033820 (2017).

[38] H. Xiong, L. G. Si, and Y. Wu, Precision measurement of electrical charges in an optomechanical system beyond linearized dynamics, Appl. Phys. Lett. **110**, 171102 (2017).

[39] Y. H. Zhou, S. S. Zhang, H. Z. Shen, and X. X. Yi, Second-order nonlinearity induced transparency, Opt. Lett. **42**, 1289 (2017).

[40] K. Børkje, A. Nunnenkamp, J. D. Teufel, and S. M. Girvin, Signatures of Nonlinear Cavity Optomechanics in the Weak Coupling Regime, Phys. Rev. Lett. **111**, 053603 (2013).

[41] Z. X. Liu, H. Xiong, and Y. Wu, Generation and amplification of a high-order sideband induced by two-level atoms in a hybrid optomechanical system, Phys. Rev. A **97**, 013801 (2018).

[42] Z. X. Liu, B.Wang, C. Kong, H. Xiong, and Y. Wu, Highly sensitive optical detector for precision measurement of Coulomb coupling strength based on a double-oscillator optomechanical system, IEEE Photon. J. **10**, 6500111 (2018).

[43] T. J. Kippenberg, H. Rokhsari, T. Carmon, A. Scherer, and K. J. Vahala, Analysis of Radiation-Pressure Induced Mechanical Oscillation of an Optical Microcavity, Phys. Rev. Lett. **95**, 033901 (2005).

[44] B. P. Hou, L. F. Wei, and S. J. Wang, Optomechanically induced transparency and absorption in hybridized optomechanical systems, Phys. Rev. A **92**, 033829 (2015).

[45] S. Liu, W. X. Yang, Z. Zhu, T. Shui, and L. Li, Quadrature squeezing of a higher-order sideband spectrum in cavity optomechanics, Opt. Lett. **43**, 9 (2018).

[46] C. Bai, B. P. Hou, D. G. Lai, and D. Wu, Tunable optomechanically induced transparency in double quadratically coupled

optomechanical cavities within a common reservoir, Phys. Rev. A **93**, 043804 (2016).

[47] H. Xiong, L. G. Si, A. S. Zheng, X. Yang, and Y. Wu, Higher-order sidebands in optomechanically induced transparency, Phys. Rev. A **86**, 013815 (2012).

[48] H. Jing, Ş. K. Özdemir, Z. Geng, J. Zhang, X. Y. Lü, B. Peng, L. Yang, and F. Nori, Optomechanically-induced transparency in parity-time-symmetric microresonators, Sci. Rep. **5**, 9663 (2015).

[49] T. Oishi and M. Tomita, Inverted coupled-resonator-induced transparency, Phys. Rev. A **88**, 013813 (2013).

[50] B. Peng, Ş. K. Özdemir, F. Lei, F. Monifi, M. Gianfreda, G. L. Long, C. M. Bender, and L. Yang, Parity-time-symmetric whispering-gallery microcavities, Nat. Phys. **10**, 394 (2014).

[51] D. Englund, A. Faraon, I. Fushman, N. Stoltz, P. Petroff, and J. Vučković, Controlling cavity reflectivity with a single quantum dot, Nature (London) **450**, 857 (2007).

[52] T. Volz, A. Reinhard, M. Winger, A. Badolato, K. J. Hennessy, E. L. Hu, and A. Imamoğlu, Ultrafast all-optical switching by single photons, Nat. Photon. **6**, 607 (2012).

[53] R. Bose, D. Sridharan, H. Kim, G. S. Solomon, and E. Waks, Low-Photon-Number Optical Switching with a Single Quantum Dot Coupled to a Photonic Crystal Cavity, Phys. Rev. Lett. **108**, 227402 (2012).

[54] A. Reinhard, T. Volz, M. Winger, A. Badolato, K. J. Hennessy, E. L. Hu, and A. Imamoğlu, Strongly correlated photons on a chip, Nat. Photon. **6**, 93 (2012).

[55] T. G. Tiecke, J. D. Thompson, N. P. de Leon, L. R. Liu, V. Vuletić, and M. D. Lukin, Nanophotonic quantum phase switch with a single atom, Nature (London) **508**, 241 (2014).

[56] V. Loo, C. Arnold, O. Gazzano, A. Lemaître, I. Sagnes, O. Krebs, P. Voisin, P. Senellart, and L. Lanco, Optical Nonlinearity for Few-Photon Pulses on a Quantum Dot-Pillar Cavity Device, Phys. Rev. Lett. **109**, 166806 (2012).

[57] S. Hughes and C. Roy, Nonlinear photon transport in a semiconductor waveguide-cavity system containing a single quantum dot: An harmonic cavity-QED regime, Phys. Rev. B **85**, 035315 (2012).

[58] H. Luo, K. Li, D. Zhang, T. Gao, and K. Jiang, Multiple sideband generation for two-frequency components injected into a tapered amplifier, Opt. Lett. **38**, 1161 (2013).

[59] L. Chang, X. Jiang, S. Hua, C. Yang, J. Wen, L. Jiang, G. Li, G. Wang, and M. Xiao, Parity-time symmetry and variable optical isolation in active-passive-coupled microresonators, Nat. Photon. **8**, 524 (2014).